

# Frustrated Cooper pairing and the $f$ -wave supersolidity

Hsiang-Hsuan Hung,<sup>1</sup> Wei-Cheng Lee,<sup>1</sup> and Congjun Wu<sup>1</sup>

<sup>1</sup>*Department of Physics, University of California, San Diego, CA 92093*

(Dated: October 29, 2018)

Geometric frustration in quantum magnetism refers to that magnetic interactions on different bonds cannot be simultaneously minimized. Usual Cooper pairing systems favor uniform spatial distributions of pairing phases among different lattice sites without frustration. In contrast, we propose “frustrated Cooper pairing” in non-bipartite lattices which leads to the supersolid states of Cooper pairs. Not only the amplitudes of the pairing order parameter but also its signs vary from site to site. This exotic pairing state naturally occurs in the  $p$ -orbital bands in optical lattices with ultra-cold spinless fermions. In the triangular lattice, it exhibits an unconventional supersolid state with the  $f$ -wave symmetry.

PACS numbers: 03.75.Ss, 75.50.Cc, 03.75.mn, 71.10.Fd, 05.50.+q

## I. INTRODUCTION

Frustration is one of the fundamental challenges in classic and quantum magnetism<sup>1</sup>. For the antiferromagnetic states in non-bipartite lattices, such as triangular, Kagome and pyrochlore, it is impossible to simultaneously minimize the magnetic energy of each bond. Consequentially, the ground state configurations are heavily degenerate. The enhanced thermal and quantum fluctuations strongly suppress spin ordering. The ultimate orderings often occur at much lower temperatures than the energy scale of the antiferromagnetic coupling through the “order from disorder mechanism”<sup>2,3</sup>. Furthermore, frustration provides a promising way to reach the spin liquid states, which exhibit exotic properties including topological ordering and fractionalization<sup>4,5</sup>.

In the usual superfluid states of paired fermions and bosons, a uniform distribution of the superfluid phase over the lattice sites is favored in order to maximally facilitate phase coherence. However, frustration can indeed occur under certain conditions. It has been found that in the disordered superconductors near the superconductor-insulator transition, the fluctuations of the superfluid density can result in frustrated Josephson coupling among superconducting grains<sup>6–8</sup>. Recently, the striped superconductivity<sup>9,10</sup> has been proposed for the high  $T_c$  compound  $\text{La}_{2-x}\text{Ba}_x\text{CuO}_4$ . The Josephson coupling between two adjacent superconducting stripes is like in the  $\pi$ -junction leading to the opposite signs of the pairing phases across the junction. The mechanism for the frustrated coupling arises from the interplay between superconductivity and antiferromagnetism in doped Mott insulators. However, an intuitive picture of the microscopic origin of this exotic phase is still needed.

On the other hand, cold atom optical lattices have opened up a new opportunity to investigate novel features of orbital physics which do not exhibit in usual orbital systems of transition metal oxides. Bosons have been pumped into the excited  $p$ -orbital bands experimentally with a long life time<sup>11–13</sup>. This metastable excited

state of bosons does not obey the “no-node” theory and exhibits the unconventional superfluidity with complex-valued many-body wavefunctions breaking time-reversal symmetry spontaneously<sup>14–17</sup>, which has already been observed<sup>12,13</sup>. For orbital fermions, large progress has been made in the  $p_{x,y}$ -orbital bands in the hexagonal lattices, whose physics is fundamentally different from that in the  $p_z$ -orbital system of graphene. The interesting physics includes the flat band structure<sup>18</sup>, the consequential non-perturbative strong correlation effects (e.g. Wigner crystal<sup>19</sup> and ferromagnetism<sup>20</sup>), frustrated orbital exchange interaction<sup>21</sup>, quantum anomalous Hall effect<sup>22</sup>, and the unconventional  $f$ -wave Cooper pairing<sup>23</sup>.

We are interested in bridging the above important research directions together by introducing frustration to Cooper pairing as a new feature of orbital physics. In this article, we propose the “frustrated Cooper pairing” in the  $p_{x,y}$ -band of the non-bipartite optical lattices with spinless fermions. Due to the odd parity nature of the  $p_{x,y}$ -orbitals, the Josephson coupling of the on-site Cooper pairing is frustrated. In the strong coupling limit, the super-exchange interaction of the pseudo-spin algebra composed of the pairing and density operators is described by the “antiferromagnetic” Heisenberg model with the Ising anisotropy. It results in the coexistence of charge density wave and superfluidity of Cooper pairs with a non-uniform phase pattern. This supersolid state of Cooper pairs exhibits the  $f$ -wave pairing symmetry in the triangular lattice within a large range of particle density.

Before we move on, let us explain some conceptual subtleties. One might wonder how to justify the validity of “frustration” of Cooper pairs which are usually an extended objects. Indeed, frustration is mostly commonly defined in antiferromagnetism of local spin moments. However, frustration does not necessarily mean “on-site” physics even in the context of antiferromagnetism in non-bipartite lattices. For example, antiferromagnetic orders can be considered as pairing between particles and holes in the spin triplet channel carrying nonzero momentum, *i.e.*, spin density waves. In the strong coupling limit, the

particle-hole pairs are strongly bound to be on-site, then the physics reduces to local moments described by the Heisenberg model. However, in the weak and intermediate coupling regimes with small charge gaps, the systems are still locally itinerant. The spatial extensions of the particle-hole bound states are beyond one lattice site. If the lattice is non-bipartite, we still have frustrated magnetism with extended particle-hole pairs. For example, this picture applies to the intermediate coupling regime of the Hubbard model at half-filling in the triangular lattice. In our case, we will consider the Cooper pairing at intermediate and strong coupling regimes. In the strong coupling limit, Cooper pairs are bound on a single site, whose exchange physics can be described by the antiferromagnetic pseudospin Heisenberg model in the charge channel. In the intermediate coupling regime, although a Cooper pair is an extended objects covering several lattice constants, its location can still be defined by its center of mass. The associated physical quantity is the pairing order parameter at each lattice site in the mean-field theory. This physics can be best explained in terms of the anomalous Green's function  $F(\vec{R}, \vec{r}; \omega)$ , where  $\vec{R}$  is the center of mass coordinate, and  $\vec{r}$  is the relative coordinate. The order parameter  $\Delta(\vec{R})$  corresponds to  $F(\vec{R}, 0; \omega = 0)$ , while the size of Cooper pairing is determined by the decay length of  $F(\vec{R}, \vec{r}; \omega = 0)$  with respect to  $r$ . In our context, frustration refers to center of mass motion of  $\Delta(\vec{R})$ .

This paper is organized as follows. The model Hamiltonian and the band structure are introduced in Sect. II. The strong coupling analysis is given in Sect. III. The mean-field theory analysis is presented in Sect. IV, and the  $f$ -wave supersolid state is presented in V. Conclusions are given in Sect. VI.

## II. THE MODEL HAMILTONIAN

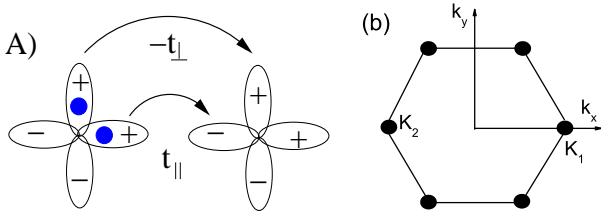


FIG. 1: (a) The  $\sigma$ -bonding and  $\pi$ -bonding of the  $p$ -orbitals have opposite signs due its odd parity nature. This gives rise to the ‘antiferromagnetic’-like exchange in the charge channel with attractive interactions as expressed in Eq. 8, which is frustrated in the triangular lattice. (b) The first Brillouin zone of the triangular lattice is a regular hexagon.  $K_{1,2} = (\pm \frac{4\pi}{3a}, 0)$  represent two non-equivalent vertices, and other four are equivalent to  $K_{1,2}$ .

We take the 2D triangular lattice as an example, which has been constructed experimentally by three coplanar

laser beams<sup>24</sup>. The optical potential on each site is approximated by a 3D anisotropic harmonic potential with frequencies  $\omega_z \gg \omega_x = \omega_y$ . After the lowest  $s$ -band is fulfilled, the active orbital bands become  $p_{x,y}$ . The  $p_z$ -band remains empty and is neglected. The free part of the  $p_{x,y}$ -orbital band Hamiltonian in the triangular lattice filled with spinless fermions reads

$$H_0 = t_{\parallel} \sum_{\vec{r}, i=1 \sim 3, \sigma} \left( p_{L, \vec{r}, i}^{\dagger} p_{L, \vec{r} + a \hat{e}_i, i} + h.c. \right) - t_{\perp} \sum_{\vec{r}, i=1 \sim 3, \sigma} \left( p_{T, \vec{r}, i}^{\dagger} p_{T, \vec{r} + a \hat{e}_i, i} + h.c. \right) - \mu \sum_{\vec{r} \sigma} n_{\vec{r} \sigma}, \quad (1)$$

where  $\vec{r}$  runs over all the sites;  $\hat{e}_1 = \hat{e}_x$ ,  $\hat{e}_{2,3} = -\frac{1}{2}\hat{e}_x \pm \frac{\sqrt{3}}{2}\hat{e}_y$  are the three unit vectors along bond directions.  $p_{L,i} \equiv (p_x \hat{e}_x + p_y \hat{e}_y) \cdot \hat{e}_i$  are the longitudinal projections of the  $p$ -orbitals along the  $\hat{e}_i$  direction. More explicitly,  $p_{L,1} = p_x$  and  $p_{L,2(3)} = -\frac{1}{2}p_x \pm \frac{\sqrt{3}}{2}p_y$ . The transverse projections of the  $p$ -orbitals along the bond read  $p_{T,i} \equiv (p_x \hat{e}_x + p_y \hat{e}_y) \cdot (\hat{z} \times \hat{e}_i)$ .  $n_{\vec{r}} = p_x^{\dagger} p_x + p_y^{\dagger} p_y$  is the particle number operator;  $\mu$  is the chemical potential. The  $\sigma$ -bonding  $t_{\parallel}$  and  $\pi$ -bonding  $t_{\perp}$  describe the hoppings between  $p$ -orbitals along and perpendicular to the bond direction, respectively, as depicted in Fig. 1 A.  $t_{\parallel}$  is positive due to the odd parity nature of the  $p$ -orbitals, which is scaled 1 below.  $t_{\perp}$  is usually much smaller than  $t_{\parallel}$  because of the anisotropy of the  $p$ -orbitals. The first Brillouin zone (BZ) of the triangular lattice is a regular hexagon as plotted in Fig. 1 B. The edge length of the first BZ is  $\frac{4\pi}{3a}$ , where  $a$  is the lattice constant.

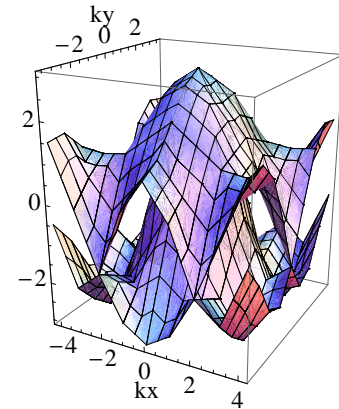


FIG. 2: The Band structure of the Hamiltonian Eq. 1. Two bands touch at  $K_{1,2}$  with the Dirac spectra, and at the center of the BZ with the quadratic spectra.

The band structure of the noninteracting Hamiltonian Eq. 1 is displayed in Fig. 2 with the value of  $t_{\perp}/t_{\parallel}$  chosen as 0.2. The band width is around  $6t_{\parallel}$ . There is no particle-hole symmetry with respect to the zero-energy point, which hints an asymmetric phase diagram with respect to half-filling for the interacting Hamiltonian

introduced in Sect. III. In momentum space, we define the two-component spinor  $\psi(\vec{k}) = (p_x(\vec{k}), p_y(\vec{k}))^T$  for the  $p_x$  and  $p_y$ -orbitals. The Hamiltonian Eq. 1 becomes

$$H = \sum_{\vec{k}} \psi_{\alpha}^{\dagger}(\vec{k}) \left\{ H_{\alpha\beta}(\vec{k}) - \mu \delta_{\alpha\beta} \right\} \psi_{\beta}(\vec{k}), \quad (2)$$

where the matrix kernel  $H_{\alpha\beta}(\vec{k})$  takes the structure of

$$H(\vec{k}) = f(\vec{k}) + g_1(\vec{k})\tau_1 + g_3(\vec{k})\tau_3, \quad (3)$$

where  $\tau_{1,3}$  are the Pauli matrices defined for the basis of  $p_x, p_y$  for the spinor of  $\psi(\vec{k})$ ; the expressions of  $f(\vec{k})$ ,  $g_1(\vec{k})$  and  $g_2(\vec{k})$  are

$$\begin{aligned} f(\vec{k}) &= (1 - t_{\perp}) \sum_i \cos \vec{k} \cdot \hat{e}_i, \\ g_1(\vec{k}) &= -\frac{\sqrt{3}}{2}(1 + t_{\perp})(\cos \vec{k} \cdot \hat{e}_2 - \cos \vec{k} \cdot \hat{e}_3), \\ g_2(\vec{k}) &= -\frac{1}{2}(1 + t_{\perp})(\cos \vec{k} \cdot \hat{e}_2 + \cos \vec{k} \cdot \hat{e}_3), \\ &\quad + (1 + t_{\perp}) \cos \vec{k} \cdot \hat{e}_1. \end{aligned} \quad (4)$$

The diagonalization of  $H(\vec{k})$  gives rise the dispersions of two bands as

$$\begin{aligned} E_{\pm} &= f(\vec{k}) \pm (1 + t_{\perp}) \\ &\quad \times \sqrt{\sum_i \cos^2 \vec{k} \cdot \hat{e}_i - \sum_{1 \leq a < b \leq 3} \cos \vec{k} \cdot \hat{e}_a \cos \vec{k} \cdot \hat{e}_b}. \end{aligned} \quad (5)$$

These two bands touch each other at  $K_{1,2}$  with the Dirac cone-like spectra, and at the center of the BZ with the quadratic spectra. When the Fermi energy is located at the Dirac points, the other band contributes a large connected branch Fermi surface, thus its contributions to thermodynamic quantities dominate over those from the Dirac points.

The topology of the Fermi surfaces varies at different filling levels. The energy minima of Eq. 1 are three-fold degenerate located at the middle points of the BZ edges. The middle points of the opposite edges are equivalent up to a reciprocal lattice vector. Around the band bottom, the Fermi surfaces only cut the first band and form three disconnected elliptical pockets. As filling increases, these pockets become connected forming a large Fermi surface around the center of the BZ. At the same time, the two Dirac cones contribute two Fermi surfaces around the  $K_{1,2}$  points, which shrink to two points when Fermi energy is right at the Dirac points. As approaching the band top where a quadratic band touching exists, there are two Fermi surfaces around the center of the BZ.

### III. STRONG COUPLING ANALYSIS

It is well-known that in the Mott-insulating state of the positive- $U$  Hubbard model at half-filling, its low energy physics lie in the magnetic channel, which is captured by the antiferromagnetic Heisenberg model<sup>25</sup>. In

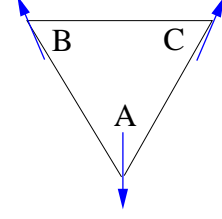


FIG. 3: The pattern of  $\langle G|\eta|G \rangle$  at  $h = 0$ : the unit cell of three sites exhibiting the supersolid ordering.

non-bipartite lattices (e.g. the triangular lattice), the antiferromagnetic exchange cannot be simultaneously minimized for every bond, which leads to frustration. Similarly, for the negative- $U$  Hubbard model, in the strong coupling limit, the low energy physics is described by the exchange interaction in the charge channel. On each site, the low energy states are the doubly occupied state and the empty state, which can be considered the pseudospin “up” and “down” state, respectively<sup>26</sup>. The Josephson coupling between neighboring sites plays the role of the ferromagnetic coupling in the  $xy$ -direction of the pseudospin, which favors a uniform phase distribution. In other words, the exchange interaction in the charge channel is unfrustrated.

This situation is fundamentally changed for the Hubbard model of spinless fermions in  $p_{x,y}$ -orbitals based on the band structure in Eq. 1. We add the attractive Hubbard interaction between spinless fermions in the  $p_{x,y}$ -orbital bands

$$H_{int} = -U \sum_{\vec{r}} n_{\vec{r},p_x} n_{\vec{r},p_y}, \quad (6)$$

where  $U$  is positive. The frustrated nature of Cooper pairing can be easily explained in the strong coupling limit of  $U \gg t_{\parallel}$ . Similarly to the usual negative  $U$  Hubbard model, we construct the pseudospin algebra denoted<sup>25</sup> as

$$\begin{aligned} \eta_x &= \frac{1}{2}(p_x^{\dagger}p_y^{\dagger} + p_y p_x), \quad \eta_y = -\frac{i}{2}(p_x^{\dagger}p_y^{\dagger} - p_y p_x), \\ \eta_z &= \frac{1}{2}(n_{\vec{r}} - 1). \end{aligned} \quad (7)$$

Up to a normalization factor, they are the real and imaginary parts of the pairing operator, and the particle density operator, respectively. The low energy Hilbert space in each site consists of the doubly occupied state and the empty state, which are eigenstate of  $\eta_z$  with eigenvalues  $\pm \frac{1}{2}$ , respectively.

This super-exchange interaction of the pseudo-spin has a remarkable feature that a  $\pi$ -phase difference is favored between pairing order parameters  $\eta_{x,y}$  on neighboring sites. As a pair hops to the neighboring site, it gains a  $\pi$ -phase shift, because the  $\sigma$ -bonding and  $\pi$ -bonding terms are with opposite signs as depicted in Fig. 1 A. The perturbation theory gives rise to the anisotropic “antiferromagnetic” Heisenberg model (AAFHM) in the “external

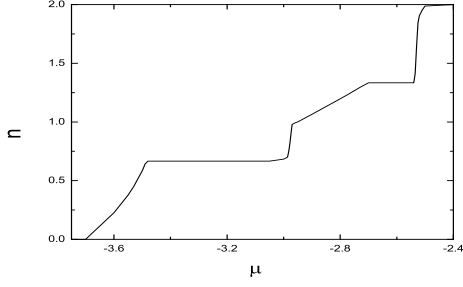


FIG. 4: The average fermion number per site  $n$  versus the chemical potential  $\mu$  at  $U/t_{\parallel} = 6$  and  $t_{\perp}/t_{\parallel} = 0.2$ .

magnetic field”,

$$H_{eff} = \sum_{ij} J_{x,y} \{ \eta_x(i) \eta_x(j) + \eta_y(i) \eta_y(j) \} + J_z \eta_z(i) \eta_z(j) - h \sum_i \eta_z(i), \quad (8)$$

where  $h = 2\mu$  is the external magnetic field; the exchange constants  $J_{x,y}$  and  $J_z$  read

$$J_{x,y} = \frac{4t_{\perp}t_{\parallel}}{U}, \quad J_z = \frac{2(t_{\perp}^2 + t_{\parallel}^2)}{U}. \quad (9)$$

The Ising anisotropy in Eq. 8 is because  $J_z \geq J_{x,y}$ . Similar models apply to pairing problem of spinless fermions in the  $p_{x,y}$ -orbital of the bipartite lattices of square<sup>27</sup> and hexagonal<sup>28</sup> which are not frustrated because a canonical transformation can change  $J_{x,y}$  to  $-J_{x,y}$ .

Eq. 8 can be interpreted as a hard core boson model with the frustrated hopping  $J_{x,y}$  and the nearest neighbor repulsion  $J_z$ . It has been studied at the zero external field in Ref. 29,30 which shows a supersolid ordering<sup>31,32</sup> with a three-site unit cell as depicted in Fig. 3. The competition between charge density wave and supersolid ordering in optical lattices has also been studied in Refs. [33,34]. Site  $A$  has no superfluid component, *i.e.*,  $\vec{\eta} \parallel \hat{z}$ ; sites  $B$  and  $C$  develop superfluid orders with a  $\pi$ -phase difference. However, the experimental realization of hard core bosons with frustrated hopping is difficult. In comparison, our idea of the frustrated Cooper pairing of fermions is very natural in the  $p_{x,y}$ -orbital bands. Furthermore, previous studies<sup>29,30</sup> focus on the pseudo-spin model Eq. 8 completely neglecting the fermion degree of freedom. In the following, instead of using Eq. 8, we directly study the Cooper pairing problem with the fermion Hamiltonian in the entire filling range from 0 to 2.

#### IV. MEAN-FIELD THEORY AT INTERMEDIATE COUPLINGS

Below we will focus on the intermediate coupling regime and perform the self-consistent mean-field theory to the fermionic Hubbard model of Eq. 1 and Eq.

6. Unlike the positive- $U$  Hubbard model with doping, in which the mean-field theory is unreliable, in our case of negative- $U$  Hubbard model, the mean-field theory gives qualitatively correct results for the competition between Cooper pairing and charge density wave (CDW). For a detailed review, please refer to Ref. 26.

To decouple  $H_{int}$ , we assume the pairing and CDW ordering taking an enlarged unit cell of three sites, and define

$$\Delta_I = \langle G | p_{\vec{r} \in I, y} p_{\vec{r} \in I, x} | G \rangle, \quad N_I = \frac{1}{2} \langle G | \hat{n}_{\vec{r} \in I} | G \rangle, \quad (10)$$

where  $I = A, B, C$  refer to the sublattice index;  $\langle G | \dots | G \rangle$  means the average over the mean-field ground state. The mean-field interaction Hamiltonian becomes:

$$H_{int}^{mf} = -U \sum_{\vec{r}, I=A,B,C} \{ \Delta_I^* p_{\vec{r} \in I, y} p_{\vec{r} \in I, x} + h.c \} + N_I \{ p_{\vec{r} \in I, x}^{\dagger} p_{\vec{r} \in I, x} + p_{\vec{r} \in I, y}^{\dagger} p_{\vec{r} \in I, y} \} \quad (11)$$

Combining Eqs. 1 and 11 and performing Fourier transformation to momentum space, we can obtain the resulting mean-field Hamiltonian as:

$$H = \sum_{\vec{k}} \hat{\Psi}^{\dagger}(\vec{k}) \begin{pmatrix} \hat{H}_s(\vec{k}) & \hat{D}(\vec{k}) \\ \hat{D}^{\dagger}(\vec{k}) & -\hat{H}_s^*(-\vec{k}) \end{pmatrix} \hat{\Psi}(\vec{k}) \quad (12)$$

where  $\sum'_{\vec{k}}$  means the summation only cover half of the reduced Brillouin zone;  $\hat{\Psi}(\vec{k})$  is defined as

$$\hat{\Psi}(\vec{k}) = (\phi(\vec{k})^T, \phi(-\vec{k})^{\dagger}), \quad (13)$$

where  $\phi(\vec{k}) = [p_{A,x}(\vec{k}), p_{A,y}(\vec{k}), p_{B,x}(\vec{k}), p_{B,y}(\vec{k}), p_{C,x}(\vec{k}), p_{C,y}(\vec{k})]$ ;  $H_s$  contains the free Hamiltonian Eq. 1 combined with the CDW decoupling;  $D(\vec{k})$  is the pairing part. The order parameters are obtained self-consistently. The above definition of order parameters are related to the pseudospin operators through

$$\begin{aligned} \langle G | \eta_x(\vec{r} \in I) | G \rangle &= \text{Re} \Delta_I, & \langle G | \eta_y(\vec{r} \in I) | G \rangle &= \text{Im} \Delta_I, \\ \langle G | \eta_z(\vec{r} \in I) | G \rangle &= N_I - 1/2. \end{aligned} \quad (14)$$

Different from the ordinary BCS problem, the pairing of Eq. 1 is not an infinitesimal instability but occurs at the finite attraction strength. It is because the eigenstates of the two time-reversal partners with momentum  $\vec{k}$  and  $-\vec{k}$  of the free Hamiltonian Eq. 1 have the same real polar orbital configuration. This suppresses pairing at weak interactions because attraction only exists in orthogonal orbitals. With intermediate and strong interactions, pairing can occur between different bands. Below we present results for  $t_{\perp}/t_{\parallel} = 0.2$  and an intermediate coupling and  $U/t_{\parallel} = 6$ . This corresponds to the effective AAFHM with the Ising anisotropy of  $J_z/J_{x,y} = 2.6$ .

We discuss our mean-field results in terms of the pseudospin orientations at the three sublattices  $A, B, C$ . Fig. 4 shows the total fermion number per site  $n = (n_A + n_B +$

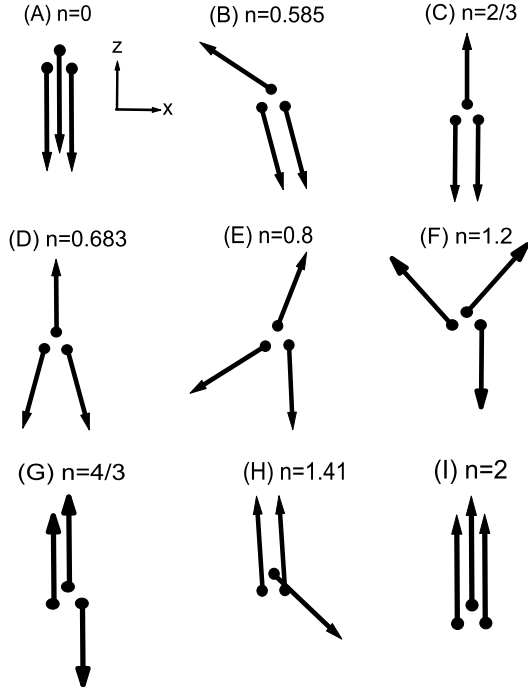


FIG. 5: The real space configurations of pseudospin  $\vec{\eta}$  on the  $xz$  plane at various fillings  $n$  from (A) to (I). (A) and (I) indicate fully polarized states. (B) and (H) show three tilted vectors, where two of them have a relative  $\pi$ -phase to the third one. (C) and (G) depict the CDW insulating state. (D) and (F) exhibit an umbrella-like shape with opposite orientation. Two of them have a  $\pi$ -phase difference and the third one does not own superfluid component. (E) denotes an intermediate configuration between (D) and (F).

$n_C)/3$  as a function of chemical potential  $\mu$ , which is the counterpart of the magnetization in the AAFHM. The first prominent feature is the plateaus occurring at  $n = \frac{2}{3}$  and  $\frac{4}{3}$ , which is corresponding to those at  $\langle G|\eta_z|G \rangle = \pm \frac{1}{3}$  observed in the study of classical ground state of the AAFHM. These two plateaus are corresponding to CDW insulating states without superfluidity. As shown in Fig. 5, the corresponding pseudospin orientation for CDW insulating states is that all the pseudospins are fully polarized along the  $\hat{z}$  axis with two of sublattice along the same direction and the remaining one along the opposite direction.

Although Fig. 4 resembles the behaviors of the magnetization obtained by the AAFHM<sup>35</sup>, two major differences exist. First, the widths of the two CDW plateaus in Fig. 4 are different while those of the AAFHM are the same. We attribute this discrepancy to the different symmetry properties between the AAFHM and the Hubbard model of Eq. 1 and Eq. 6 with the asymmetric band structure shown in Fig. 2. The AAFHM has the symmetry of the rotation of  $180^\circ$  around the  $x$ -axis, *i.e.*,  $\eta_x \rightarrow \eta_x$ ,  $\eta_y, \eta_z \rightarrow -\eta_y, -\eta_z$  and  $h \rightarrow -h$ . Such an operator corresponds to the particle-hole transformation at the fermion level as  $p_x \rightarrow ip_y^\dagger$  and  $p_y^\dagger \rightarrow ip_x$ , which

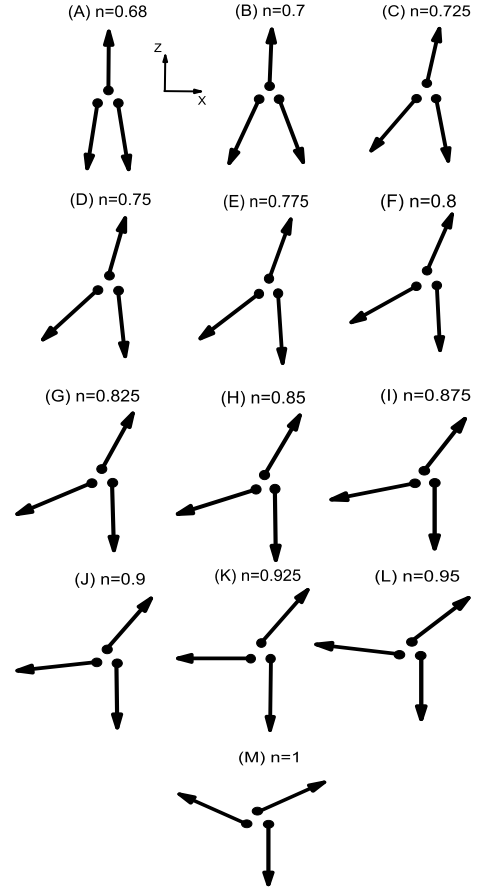


FIG. 6: The smooth evolution of the two opposite “umbrella”-like configurations from  $n = 0.68$  to  $n = 1$ .

is not kept in the triangular lattice. As a result, for the AAFHM, the magnetization should be an odd function with respect to  $h$  so that the lengths of the plateaus are the same. This kind of behavior is not expected in Fig. 4. The other difference is that at  $h = 0$ , the ferrimagnetic state is found in the AAFHM, and our results show the “paramagnetic” behavior, *i.e.*, there is no jump around  $n = 1$ . This is due to the quantum fluctuations arising from the singly occupied states as discussed below.

Fig. 5 plots the pseudospin orientations on three sublattices at a series of filling levels. Except the CDW insulating states at  $n = \frac{2}{3}, \frac{4}{3}$ , we find that the pseudospins have non-zero  $\langle G|\eta_x|G \rangle$  and  $\langle G|\eta_z|G \rangle$  in the most part of the phase diagram, indicating the frustrated supersolid states with non-uniform Cooper pairing density and phase. Moreover, the phase diagram can be well-understood by the rotations of pseudospin orientation under the magnetic field  $h = 2\mu$ . At  $n = 0$ ,  $h$  is large along the  $-\hat{z}$  direction so that all the pseudospins are completely polarized. As  $n$  increases, the magnitude of  $h$  decreases so that the pseudospins gradually rotate upward with one of the pseudospins ( $\vec{\eta}(A)$ ) having much faster rotating rate. They become polarized along the  $z$ -direction as arriving at the CDW insulating state  $n = \frac{2}{3}$  with one

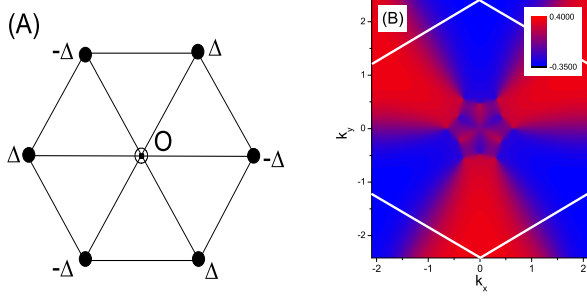


FIG. 7: The  $f$ -wave pairing pattern in (A) real space and (B) momentum space. The rotation of  $60^\circ$  around the center site  $O$  in (A) (denoted by the hollow circle) in real space or around the center of the reduced BZ in momentum space is equivalent to reverse the sign of the pairing order parameters.

pointing up and the other two pointing down. The magnitudes of  $\eta_{A,B,C}$  are smaller than  $\frac{1}{2}$  due to quantum fluctuations. As  $n$  increases further, since  $\eta^z(A)$  can not increase anymore,  $\vec{\eta}(B)$  and  $\vec{\eta}(C)$  gradually turn upward leaving  $\vec{\eta}_A$  unchanged forming an umbrella configuration. Such a state is a coexistence of superfluidity and CDW, thus is a supersolid state.

After a critical value  $n_c \sim 0.7$ , all the pseudospins start to rotate simultaneously and continuously evolve between the two umbrella configurations with opposite orientations depicted in (D) and (F) in Fig. 5, respectively. A detailed process of evolution is plotted in Fig. 6 from  $n = 0.68$  to  $n = 1$ . This continuous evolution of the ground state is not present in the AAFHM since its ground state is ferrimagnetic with non-zero magnetization at zero field, which corresponds to  $n \neq 1$  in our model. This deviation is because the AAFHAM model is only justified at the strong coupling limit. The larger kinetic energy in this region leads to the less stringent assumption of the strong-coupling. Consequently, the quantum fluctuations arising from the singly occupied states are enhanced, which are in disfavor of CDW but in favor of uniform superfluidity. The continuous evolution also explains why there is no jump at  $n = 1$  in Fig. 4. Finally, the rest part of the phase diagram can be easily understood by rotating all the pseudospins upward, and eventually all the pseudospins are fully polarized along  $+\hat{z}$  direction at  $n = 2$ .

## V. THE $f$ -WAVE SUPERSOLID STATE

One remarkable feature of the frustrated Cooper pairing that we are studying is that it can give rises to an unconventional type supersolid state exhibiting non- $s$ -wave symmetry. For example, in Fig. 5 for a wide region of  $n$  ( $0.67 \leq n \leq 0.7$ ,  $1 \leq n \leq 1.3$ ), we find  $\langle G|\eta_x(A)|G\rangle = 0$  and  $\langle G|\eta_x(B)|G\rangle = -\langle G|\eta_x(C)|G\rangle = \Delta$ . As shown in Fig. 7 A, the signs of the pairing order parameter are opposite in sublattices  $A$  and  $B$ . As a result, a spatial

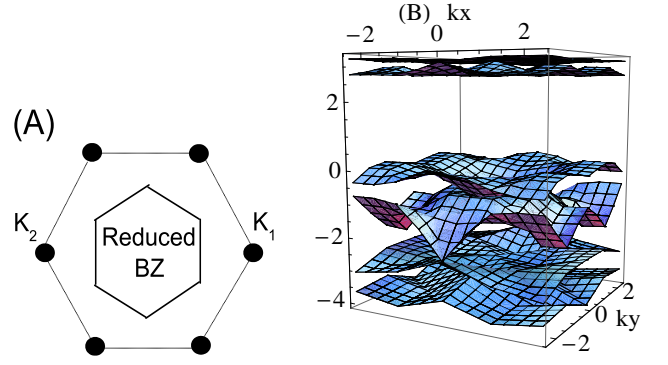


FIG. 8: A) The reduced Brillouin zone (RBZ) associated with the enlarged three-site unit cell compared with the original BZ. The six vertices of the RBZ are located at the centers of the six regular triangles composed of the center of the BZ and the vertices of the original BZ. B) The six bands in the reduced BZ with the three-site CDW pattern of  $n_A = n_C = 1.52$ , and  $n_B = 0.154$  for  $t_\perp = 0.2$  and  $U = 6$ . The chemical potential  $\mu$  is reset to zero.

rotation around a site of sublattice  $C$  at  $60^\circ$  corresponds to flipping the sign of the order parameters, which indicates the  $f$ -wave pairing symmetry.

The  $f$ -wave pairing symmetry is also manifest in the gap function structure in momentum space. We calculate the intra-band pairing functions  $\Delta_{nm}$  in the momentum space by projecting the pairing potential in Eq. 11 to the band eigen-basis as:

$$\sum_{\vec{k}} \sum_{m,n=1}^6 \Delta_{nm}^*(\vec{k}) \psi_n(\vec{k}) \psi_m(-\vec{k}) + h.c., \quad (15)$$

where

$$\Delta_{nm}(\vec{k}) = [\hat{U}^\dagger(\vec{k}) D(\vec{k}) \hat{U}^*(-\vec{k})]_{nm}, \quad (16)$$

$\hat{U}(\vec{k})$  is the unitary matrix such that

$$\hat{U}^\dagger(\vec{k}) H_s(\vec{k}) \hat{U}(\vec{k}) = \text{diag}[E_1(\vec{k}), \dots, E_6(\vec{k})], \quad (17)$$

and  $H_s(\vec{k})$ ,  $D(\vec{k})$  are given in Eq. 12. We have confirmed that all six intra-band pairing functions have three nodal lines and sign changes under  $60^\circ$  rotation.

As a specific example, we present the results of the self-consistent mean-field theory for the filling  $n = 1.07$  and other parameters  $t_\perp = 0.2$  and  $U = 6$  as before. The system exhibits the three-site pattern of the CDW order as  $n_A = n_C = 1.52$ , and  $n_B = 0.154$ , and the pairing order parameters in the real space are  $\Delta_A = -\Delta_C = 0.345$  and  $\Delta_B = 0$ . We plot the band structure with the above CDW order parameter but set the gap functions zero. The reduced BZ is only  $\frac{1}{3}$  of the original BZ, and there are six bands in total as plotted in Fig. 8. The chemical potential  $\mu$  is reset to 0, which lies in the gap between the 4th and 5th bands and has no crossing with the band spectra. As a result, although the gap functions

have node lines due to the  $f$ -wave symmetry, the Bogoliubov excitations remains fully gapped. We plot the gap function of  $\Delta_{44}$  in Fig. 7 B for demonstration purpose. The nodal lines are the three lines connecting the middle points of the opposite edges of BZ. Thus this is an unconventional supersolid state of frustrated Cooper pairing with the  $f$ -wave pairing symmetry. Another interesting feature is that the gap function  $\Delta_{44}$  even changes sign along the radial direction.

It would also be instructive to compare our  $f$ -wave pairing supersolid state of Cooper pairs with the Fulde-Ferrell-Larkin-Ovchinnikov (FFLO) state<sup>36,37</sup>. Both cases exhibit non-uniform distributions of pairing phase in real space. However, the FFLO state completely breaks rotational symmetry. Its pairing pattern does not form a well-defined representation of the lattice point group in momentum space. In our case, it has a well-defined  $f$ -wave symmetry.

We also consider the extreme anisotropy limit of the vanishing  $\pi$ -bonding strength, i.e.,  $t_{\perp} = 0$ . The bond superexchange only results in the  $J_z$ -term at the second order perturbation level in Eq. 8. The leading order of the hopping of the Cooper pairs occurs through the three-site ring exchange

$$\Delta H = - \sum_{ijk} J' [\eta_x(i)\eta_x(j) + \eta_y(i)\eta_y(j)]\eta_z(k) \quad (18)$$

where  $J' = \frac{9}{2} \frac{t_{\parallel}^3}{U}$ . The hopping is frustrated for a plaquette with only one site occupied, but it is unfrustrated for a plaquette with two sites occupied. This means that at low fillings the phase diagram does not change much from

the case of nonzero  $t_{\perp}$ , while the system finally evolves to a uniform pairing phase at  $n$  close 2. A more detailed analysis will be presented in a later publication.

## VI. CONCLUSION

In summary, we introduce the concept of “frustrated Cooper pairing” of spinless fermions in the  $p$ -orbital band in optical lattices. The frustration occurs naturally from the odd parity of the  $p$ -orbitals and is a new feature of orbital physics. Exotic supersolid states of Cooper pairs with nonuniform distributions of pair density and phase are obtained with an unconventional  $f$ -wave symmetry. This opens up a new opportunity to study the physics of frustrated magnet by using the pseudo-spin algebra of the charge and pair degrees of freedom of Cooper pairs. This idea can also be applied to other even more frustrated lattices, such as Kagome and pyrochlore. In considering the possibility of the existence of exciting spin liquid states therein, their counterparts in terms of “frustrated Cooper pairs” is another interesting direction for further exploration.

## Acknowledgments

C. W. thanks J. Hirsch for helpful discussions. C. W., H. H. H, and W. C. L are supported by NSF-DMR-0804775, and AFOSR YIP program.

*Note added* Upon the completion of this manuscript, we learned the work by Cai *et al.*<sup>38</sup> in which a similar problem in the square lattice is investigated.

- 
- <sup>1</sup> H. T. Diep, *FRUSTRATED SPIN SYSTEMS* (World Scientific, Singapore, 2005).
  - <sup>2</sup> E. F. Shender, Soviet Physics - JETP **56**, 178 (1982).
  - <sup>3</sup> C. L. Henley, Phys. Rev. Lett. **62**, 2056 (1989).
  - <sup>4</sup> G. Misguich, Quantum spin liquids, arXiv.org:0809.2257, 2008.
  - <sup>5</sup> R. Moessner and K. S. Raman, Quantum dimer models, arXiv.org:0809.2257, 2008.
  - <sup>6</sup> F. Zhou and B. Spivak, Phys. Rev. Lett. **80**, 5647 (1998).
  - <sup>7</sup> F. Zhou and C. Biagini, Phys. Rev. Lett. **81**, 4724 (1998).
  - <sup>8</sup> B. I. Spivak and S. A. Kivelson, Phys. Rev. B **43**, 3740 (1991).
  - <sup>9</sup> E. Berg, E. Fradkin, and S. A. Kivelson, Physical Review B **79**, 064515 (2009).
  - <sup>10</sup> E. Berg, E. Fradkin, S. A. Kivelson, and J. Tranquada, Striped superconductors: How the cuprates intertwine spin, charge and superconducting orders, arXiv.org:0901.4826, 2009.
  - <sup>11</sup> T. Müller, S. Fölling, A. Widera, and I. Bloch, Phys. Rev. Lett. **99**, 200405 (2007).
  - <sup>12</sup> G. Wirth, M. Ölschläger, and A. Hemmerich, Nat. Phys. **7**, 147 (2011).
  - <sup>13</sup> M. Ölschläger, G. Wirth, and A. Hemmerich, Phys. Rev. Lett. **106**, 015302 (2011).
  - <sup>14</sup> A. Isacsson and S. M. Girvin, Phys. Rev. A **72**, 053604 (2005).
  - <sup>15</sup> W. V. Liu and C. Wu, Phys. Rev. A **74**, 13607 (2006).
  - <sup>16</sup> C. Wu, W. V. Liu, J. E. Moore, and S. Das Sarma, Phys. Rev. Lett. **97**, 190406 (2006).
  - <sup>17</sup> C. Wu, Mod. Phys. Lett. B **23**, 1 (2009).
  - <sup>18</sup> C. Wu, D. Bergman, L. Balents, and S. D. Sarma, Phys. Rev. Lett. **99**, 70401 (2007).
  - <sup>19</sup> C. Wu and S. D. Sarma, Phys. Rev. B **77**, 235107 (2008).
  - <sup>20</sup> S. Zhang, H.-h. Hung, and C. Wu, Phys. Rev. A **82**, 053618 (2010).
  - <sup>21</sup> C. Wu, Phys. Rev. Lett. **100**, 200406 (2008).
  - <sup>22</sup> C. Wu, Phys. Rev. Lett. **101**, 186807 (2008).
  - <sup>23</sup> W. C. Lee, C. Wu, and S. Das Sarma, Phys. Rev. A **82**, 053611 (2010).
  - <sup>24</sup> C. Becker, P. Soltan-Panahi, J. Kronjager, S. Stellmer, K. Bongs, and K. Sengstock, *Lasers and Electro-Optics, 2007 and the International Quantum Electronics Conference*, 2007.
  - <sup>25</sup> A. Auerbach, *Interacting Electrons and Quantum Magnetism*, Springer, 1994.
  - <sup>26</sup> R. Micnas, J. Ranninger, and S. Robaszkiewicz, Rev. Mod. Phys. **62**, 113 (1990).
  - <sup>27</sup> A. E. Feiguin and M. P. A. Fisher, Phys. Rev. Lett. **103**,

- 025303 (2009).
- <sup>28</sup> W.-C. Lee, C. Wu, and S. Das Sarma, Phys. Rev. A **82**, 053611 (2010).
- <sup>29</sup> H. C. Jiang, M. Q. Weng, Z. Y. Weng, D. N. Sheng, and L. Balents, Phys. Rev. B **79**, 020409 (2009).
- <sup>30</sup> F. Wang, F. Pollmann, and A. Vishwanath, Phys. Rev. Lett. **102**, 017203 (2009).
- <sup>31</sup> A. F. Andreev and I. M. Lifshitz, Sov. Phys. JETP. **29**, 1107 (1969).
- <sup>32</sup> G. V. Chester, Phys. Rev. A **2**, 256 (1970).
- <sup>33</sup> T. L. Dao, A. Georges, and M. Capone, Phys. Rev. B **76**, 104517 (2007).
- <sup>34</sup> A. Koga, T. Higashiyama, K. Inaba, S. Suga, and N. Kawakami, Phys. Rev. A **79**, 013607 (2009).
- <sup>35</sup> S. Miyashita, J. Phys. Soc. Jpn. **55**, 3605 (1986).
- <sup>36</sup> P. Fulde, R. A. Ferrell, Phys. Rev. **135**, A550 (1964).
- <sup>37</sup> A. I. Larkin and Y. N. Ovchinnikov, Sov. Phys.- JETP **20**, 762 (1965).
- <sup>38</sup> Z. Cai, L. Wang, J. Li, S. Chen, X. C. Xie, and Y. Wang, arXiv:0910.0508 (2009).



